Proceedings of the 11th International Conference on Fluid Flow, Heat and Mass Transfer (FFHMT 2024)
Chestnut Conference Centre - University of Toronto, Toronto, Canada – June 16-18, 2024
Paper No. 045
DOI: 10.11159/ffhmt24.045

Development of an Experimental Setup for the Practical Assessment of Partially Premixed Acetylene/Air Flame Heating Processes

Christian Herwerth [1,2], Giovanni Luca Turi da Fonte Dias[1,3], Jacqueline Ungar[1], Vaibhav Kumbhar[1], Sebastian Ulmer[1], Herbert Pfeifer[2]
[1]Linde GmbH
Carl-von-Linde-Strasse 25, 85716 Unterschleissheim, Germany
christian.herwerth@linde.com
[2]RWTH Aachen University, Aachen, Germany, Faculty of Georesources and Materials Engineering, Department for Industrial Furnaces and Heat Engineering
[3]Technical University of Munich, Germany; TUM School of Natural Sciences, Department of Chemical Engineering

Abstract **–** Two experimental setups for the assessment of acetylene/compressed air flame impingement systems are developed. The first setup determines the heat transfer efficiency between a single jet flame and a target (calorimeter), while the second setup facilitates the scale-up to industrial sized torches and provides additional information about the temperature field in the target (steel plate). Qualifying experiments include studies of the heat transfer efficiency as functions of the Reynolds number and the torch-to-target distance. The observed effects are in good agreement with the available literature. In the future, the setups will be used to further study heat transfer enhancement strategies and the impact of process gas variation on the flame impingement system performance.

Keywords**:** Heat transfer, flame impingement, premixed acetylene/air combustion, flame heating

Notations

c_p	Specific heat capacity	HoC	Heat of Combustion, net calorific value	t	Time
D	Torch diameter	IQR	Interquartile range	T	Temperature
η	Efficiency	$\dot{m}$	Mass flow	$\dot{V}$	Volume flow
f	Arbitrary function	ρ	Density	V	Volume of reference element
H	Distance torch/target	σ	Standard deviation	x	Arbitrary measuring value

1. Introduction

Industrial flame heating is vital to modern manufacturing processes with applications from hardening to flame straightening. Heat transfer (HT) occurs from the flame to the target and is commonly described by the flame jet impingement model (figure 1).

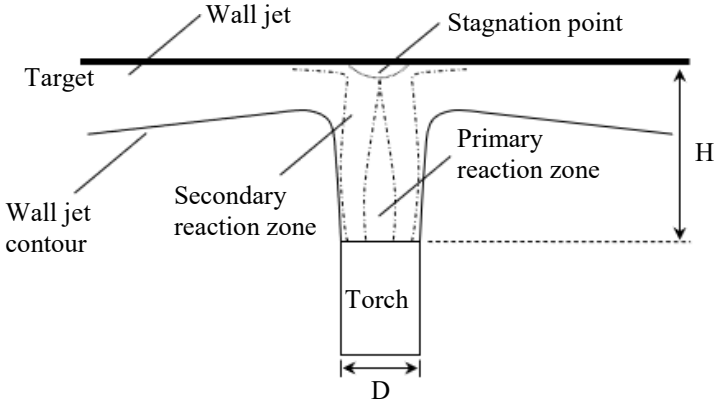

Figure 1: Hydrodynamic principles of flame impingement, HT occurs at the stagnation point and in the wall jet region.

Extensive research has focused on impingement jets for nearly 50 years, covering flow field descriptions [1], [2], turbulent structures [3] and the associated HT process [4], [5]. Researchers have provided fundamental understanding of jet flame characteristics [6] and HT mechanisms [7], and several contemporary literature and data reviews including relevant correlations are available [8], [9], [10]. In a more recent review, Chander and Ray summarize various published methods for assessing the HT numerically and experimentally [11].

Turbulence effects on stagnation point HT have been extensively studied [12], [13] and numerous research groups are exploring different methods to enhance the HT using experimental and numerical models. Passive methods, such as self-exciting set-ups [14] and nozzle manipulation [15], [16] seem more feasible for industrial flame heating purposes than active methods, such as acoustic excitation [17] imposing added complexity.

As an application, industrial flame impingement heating is often used to preheat fine-grain high-strength steels before e.g., submerged-arc welding. This helps to prevent hot and cold cracks during and after welding, particularly in components with large wall-thicknesses. Various fuel gases, usually in a slightly rich, premixed configuration with air as oxidizer are used for this application. Acetylene (C_2H_2), compared to other common fuel gases, has a significantly higher flame temperature, leading to increased heat flux [7], [18] and shorter process times, making it popular for autogenous heating technologies.

To increase the efficiency and sustainability of flame heating processes, enhancing the HT from the flame jet into the target, is a crucial task. An experimental testing setup, capable of capturing HT effects of premixed acetylene/air flame jet impingement systems has been established. The evaluation focuses on parameters relevant for industrial applications such as HT efficiency and temperature distribution in the target. Detailed descriptions of the experimental setup, data assessment, and results are presented in the following sections.

2. Material and methods

In assessing flame impingement systems, the first parameter of interest is the overall HT efficiency, representing the proportion of the released heat of combustion (HoC) transferred into the target. The experimental setup features a water-cooled copper plate/heat-exchanger (HX) [19], heated by a single flame jet. As the measurement of the spatial heat distribution is also crucial, as e.g., pre-heating for welding processes, transfers the HoC very locally into the target, a second setup for heating a solid steel body is developed. Both experimental setups share a common gas supply but differ in torch, target, and data acquisition systems. The combined setup allows fast concept testing and larger scale-up tests. The water-cooling of the calorimeter allows significantly higher test loads, enabling a good and fast assessment of the overall HT. The solid body is used for HT assessments of industrial sized torches with more power and provides further information about the temperature field. A complete piping and instrumentation diagram is depicted in figure 2.

2.1. Experimental set-up “Calorimeter”

A commercially available venturi-principle mixing nozzle/machine shaft (Linde Lindoflamm LF-S-1) is used to premix the fuel gas and oxidizer, maintaining a constant equivalence ratio. The impingement target is a water-cooled plate HX (copper, 200x200x10 mm), consisting of an 8mm thick sheet with 18 machined passages (6x6 mm) and a 2 mm cover plate. The process water is filtered, regulated (Riegler 100.53) to not exceed a relative pressure of 10^5 Pa at the HX inlet, and pre-heated to approx. 323 K (Stiebel Eltron DHB-E 24 LCD) to prevent condensation at the target. Inlet and outlet temperatures of the water flow are measured using two temperature sensors ifm TM4591, with an absolute deviation between the sensors of 0.15 K (calibration in ice water). A thermocouple (TC) mounted at the HX’s centre serves as a safeguard to prevent local boiling within the HX. The process water flow is measured using a Buerkert 8032/SE32 mass-flowmeter (MFM), calibrated to cover a flow rate of 0.03 to 0.07 l s^{-1} with approx. 0.05 l s^{-1} as the desired set-point.

2.2. Experimental set-up “Solid body”

Similar to the “calorimeter” setup, a Linde Lindoflamm LF-S-2 is used. The impingement target is a solid plate (P265 (P265 GH, 350x35 mm) with three rows of bores (diameter 2.5 mm) and different depths per row (8.8, 19.5, 26.3 mm), located on different diameters (multiples of 19.5 mm). They are each equipped with a type K thermocouple. The bore pattern pattern (figure 3) and the associated temperature measurement can be used to spatially resolve the temperature field of the the plate during the impingement heating process.

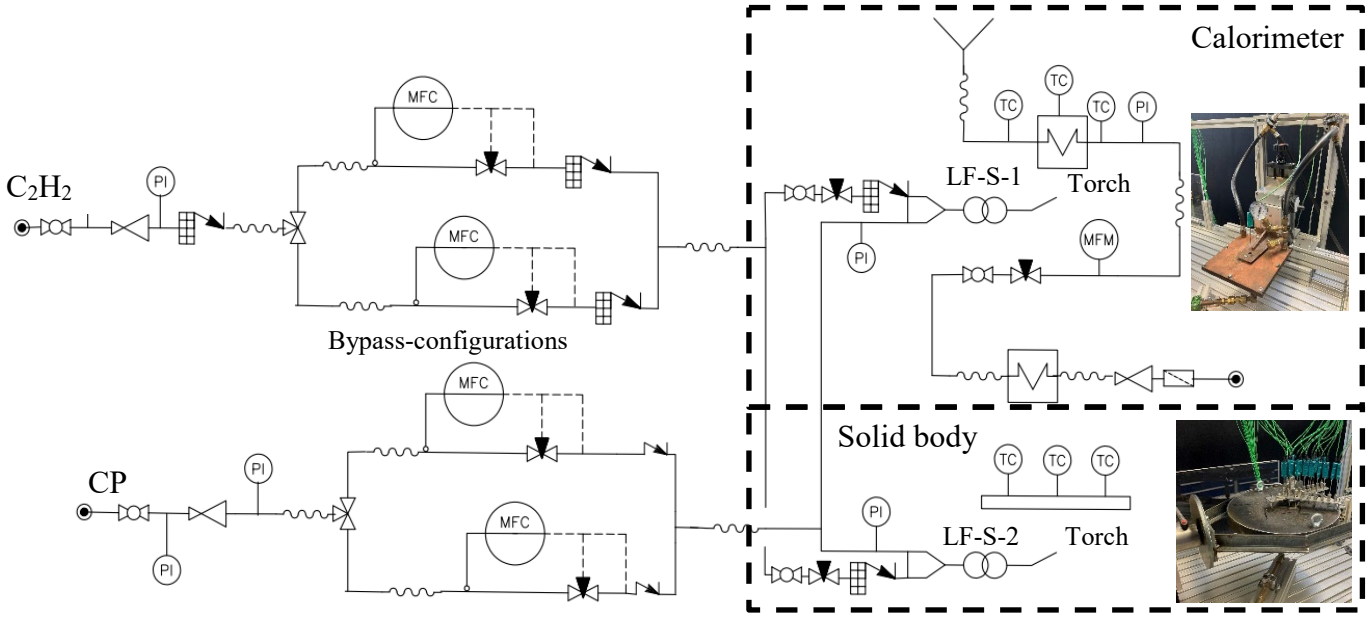

Figure 2: Each pre-mixing stage (LF-S-1/LF-S-2) is equipped with a flame arrestor (Witt 85-10) to prevent flashbacks from entering the up-stream lines. Gas flows for C_2H_2 and compressed air (CP) are measured and regulated using mass-flow-controllers (MFC, Buerkert 8741) in a bypass configuration. Check-valves (Witt Ultra 12 and Ultra 20) and flashback arrestors (Witt 85-10) were used to protect the MFCs from backflow. At the tapping point of the C_2H_2, a flashback arrestor (Witt 85-10) prevents e.g., acetylene decomposition reactions to enter the high-pressure system up-stream.

2.3. Data acquisition

The CompactDAQ series from National Instruments (NI) is used for both experimental setups. The central module is the NI CompactDAQ 9189 chassis with the required sensor-specific modules connected:

- NI-9207 (Buerkert MFCs 8741)
- NI-9211 (TC type K “calorimeter”)
- NI-9213 (TC type K “solid body”)
- NI-9216 (for ifm TM4591)
- NI-9269 (Buerkert MFCs 8741)

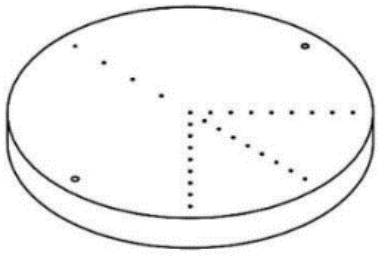

Figure 3: Schematic of the bore pattern for the solid body.

National Instrument’s LabVIEW software is used for the data acquisition. A customized VI was created using the producer/consumer architecture, facilitating an efficiently buffered communication between data acquisition and data processing loops with different frequencies. The postprocessing is conducted in Python and MATLAB.

2.4. Investigated torches

"Calorimeter" set-up

A simple circular flame jet was specified for the assessment of the experimental capabilities. The setup's ability to measure and quantify changes in heat flow was validated by using three flow rate configurations, classified by their Reynolds number (Re, table 1).

"Solid body" set-up

For the assessment and qualification of the test rig "solid body" a circular flame jet was used. The tested flow rate and the associated Re configuration is summarized in table 1.

Table 1: C_2H_2/CP flow rates and associated Reynolds numbers for the calorimeter and solid body setup.

	Reynolds number	*Flow rate C_2H_2 [Nl/min]*	*Flow rate CP [Nl/min]*
Calorimeter	2500	1.1	6.9
	5250	2.33	14.7
	8000	3.56	22.4
Solid body	8000	7.9	49.7

3. Results and discussion

The following section presents the results of the qualifying experiments investigating the efficiency and temperature distribution of acetylene/compressed air flame jet impingement systems and includes a discussion of the observed effects in comparison with previous literature findings.

3.1. Calorimeter

Each flow rate/Reynolds configuration was tested through three independent experiments for five different calorimeter/torch tip distances. After setting/adjusting the distance, a visibly stationary mode of operation was awaited before starting the time measurement. The sensors were synchronized at a frequency of 1 Hz and each measurement persisted for 240 s. Assuming a constant $c_{p,\,H2O}$ and taking the net calorific value as HoC_{C2H2}, the efficiency for each normalized distance H/D is calculated continuously using equation (1).

$$\eta = \frac{\dot{m}_{H2O} \cdot c_{p,\,H2O} \cdot (T_{Out} - T_{In})}{\dot{V}_{C2H2} \cdot HoC_{C2H2}} \tag{1}$$

The time series for each H/D is averaged during post-processing. Outliers caused by cooling water flow rate fluctuations are eliminated using a strict cut-off criterion of $\eta_{cut} = \bar{\eta} \pm 1.5\, IQR$. The specific error is derived using the Gaussian error propagation law for time series (st. dev. σ as individual error) applied to the function of equation (1).

Figure 4 shows the results of the Reynolds number variation. For all H/D, reducing the Reynolds number increases the HT efficiency. The reduced gas flow and the resulting lower wall jet velocity allows for more time to exchange energy from the flue gas to the target. Qualitative comparison of the curves for the different Re-configurations shows, that the peak efficiency for Re = 2500 occurs between H/D = 4-6. Due to the low outlet velocity, the tip of the primary reaction zone is located at a closer range to the torch, than for the increasingly turbulent flames of Re = 5250 and 8000 (photos in figure 4). The lower efficiency for the flames of Re = 5250 and 8000 at low H/D suggests the target is located within the reaction zone. Potential reasons for the low efficiencies are the entrainment of cold ambient air and additional reaction quenching in the wall-jet region around the comparably cold calorimeter surface, which prevent optimal combustion. A reduction in efficiency is observed downstream of each flame's individual performance peak due to further entrainment of cold ambient air [7]. The effect is in good agreement with existing literature: Hargrave et al. [7] reported high heat fluxes for low Re flames at short distances, whereas high Re flames show their respective peak

efficiency at increasingly larger H/D. These findings were explained with the location of the reaction zone and the associated high temperatures at its tip. Furthermore, the observed post-peak region of approx. constant efficiency for the flames of Re = 5250 and 8000 is consistent with the previously documented findings of van der Meer [13].

The propagated error was never larger than $\Delta\eta = 2.5$ % (error bars in figure 4). As the Reynolds number decreased, the error increases since errors in the water flow/temperature measurement generally have a higher impact on the determination of the efficiency for low Re flows.

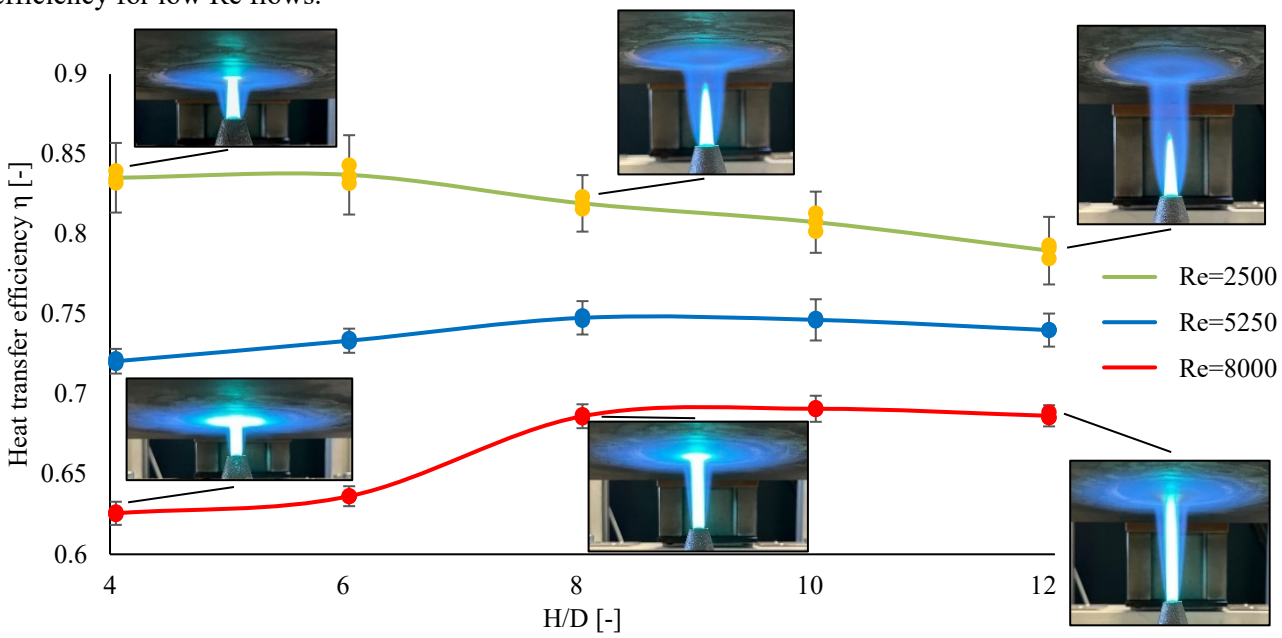

Figure 4: Flame impingement heat transfer efficiency for different Reynolds numbers and normalized distances H/D.

3.2. Solid body

Three independent experiments were conducted for each normalized distance H/D. The respective distance was set, the reaction zone was established, and the time measurement and data collection were started at a frequency of 1 Hz. To evaluate the temperature distribution, the solid body is divided into reference sections making use of the rotational symmetry of the target and the torch. With one TC assigned to each volume element, the temperature distribution for the whole target can be evaluated by extra- and interpolating. Figure 5 shows the temperature distributions for different torch/target distances after 240 s of heating and a schematic of the TC/bore pattern.

In addition to the temperature field, the unsteady HT efficiency for each timepoint t, starting with the ignition (index i) is calculated using equation (2), which also accounts for the temperature-dependency of the specific heat capacity $c_{p,\,P265GH}$ of the body.

$$\eta(t) = \frac{\sum_{n=1}^{m} \rho_{P265GH} \cdot V_m \cdot \left[\int_{T_i}^{T_t} c_{p,\,P265GH}(T)\, dT\right]_m}{\dot{V}_{C2H2} \cdot HoC_{C2H2} \cdot t} \tag{2}$$

Typical plots of $\eta(t)$ are depicted in figure 6. Starting with the ignition, the calculated efficiency rises until an approximate steady-state HT/efficiency is reached. The time before the steady-state HT must not be evaluated due to the time-dependent conductive process: Heat from the lowest plane of the plate (interface flame/target) still conducts towards the TCs while the flame is already ignited. The numerator in equation (2) lags the denominator.

In the presented experiments, the fuel gas flow endured for 240 s, with the interruption indicated by a minor hike in the efficiency curve (additional effect due to lag numerator/denominator). Shortly after the flame is extinguished the conductive process is complete and the developed inter- and extrapolation scheme for the now quasi-stationary temperature field is correct, resulting in the detected and compared peak of maximum efficiency. The gradual post-peak decrease is due to the natural convection cooling of the plate.

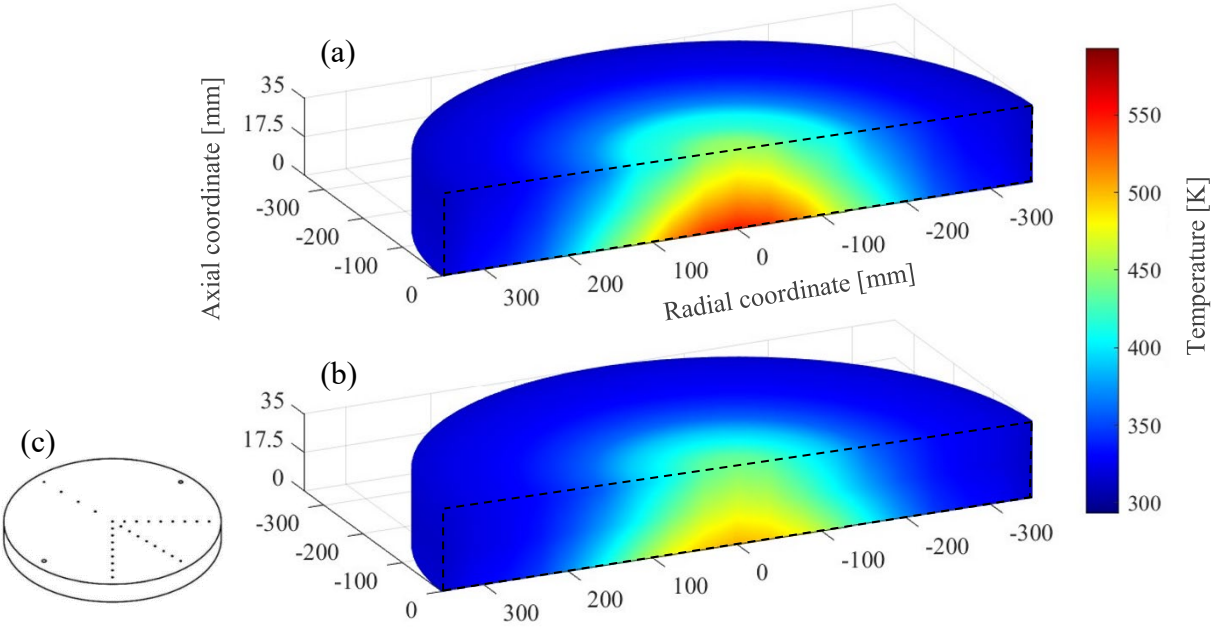

Figure 5: Effect of distance variation (a) H/D = 3 and (b) H/D = 6 on the temperature field of the test plate after 240 s of heating and schematic of the TC pattern (c).

The error for each individual temporal assessment of equation (2) is determined using the Gaussian error propagation law using the cumulative relative error Δx of each measuring chain as the individual variable error. This propagated error of $\eta = f(t)$ is mostly influenced by the error of the TC measuring chain and decreases rapidly to insignificant values ($\Delta\eta(t) < 0.5$ %) as the temperature increases. The standard deviation (illustrated as the error bar in figure 6) between identical but repeated experiments is primarily caused by varying thermal resistances between the TC and its respective bore, as well as a high distance sensitivity, notably for H/D = 3 where $\Delta\eta_{max}$ exceeded 10 % within ΔH/D = 1. As it is more relevant to assess the quality of the measuring system, than $\Delta\eta(t)$, this standard deviation σ is included as the respective error bar in figure 6. A comparison of the peak efficiency for H/D = 3 with the other investigated distances indicates a clear change in max. HT efficiency. The curves for H/D = 4, 6, 8 and 10 can hardly be distinguished, owing to the physical effect of an approx. constant efficiency region downstream of the max. efficiency [7], [13]. At H/D = 12 a significant drop in max. HT efficiency can be detected. The results for the temperature distribution as well as for the peak HT efficiencies are plausible and in good agreement with available literature [7], [13].

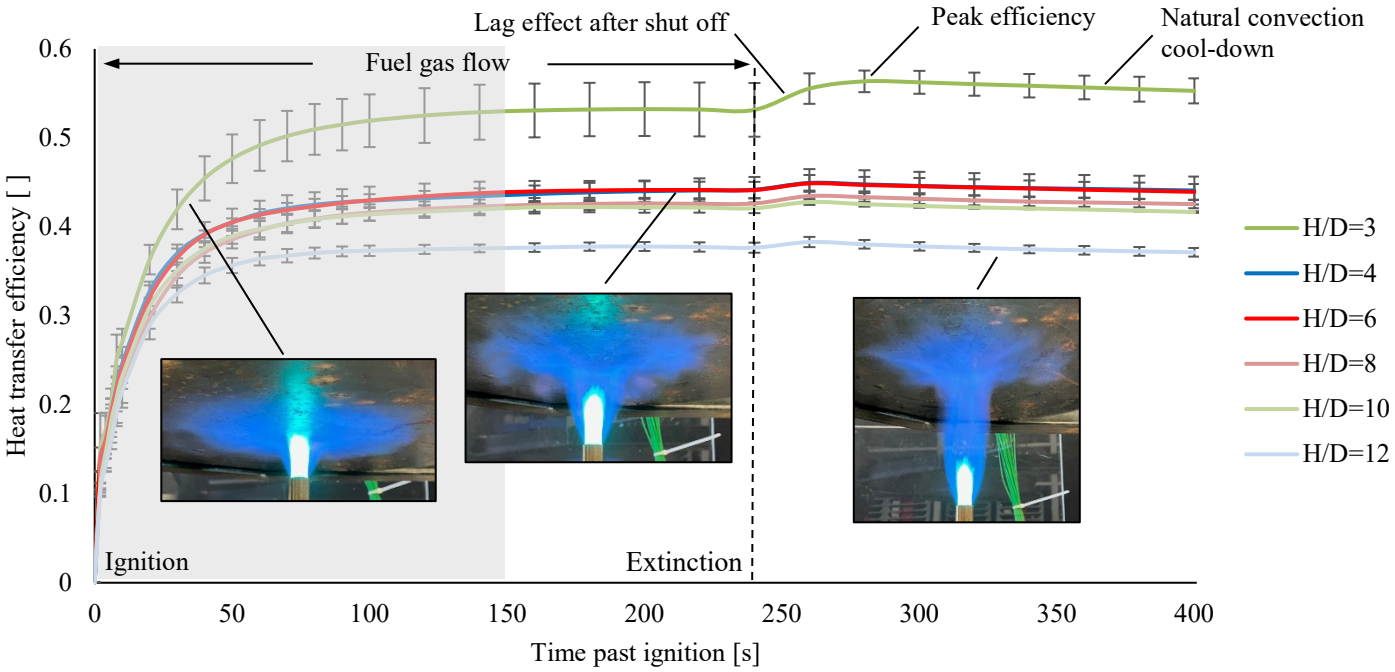

Figure 6: Effect of H/D variation on the unsteady heat transfer efficiency according to equation (2). The error bars indicate the standard deviation between the individual experiments for each H/D and the greyed-out area marks the region of increased lag error (no valid data assessment possible).

4. Conclusion

In summary, the developed test equipment can clearly distinguish between different torch efficiencies for a wide range of flow rates and torch/target distances. The test rig is fully functional, the observed effects are transferable between the setups and consistent with previously published literature findings [7], [13]. The HT efficiency measurements alone are not sufficient for evaluating proficient heating processes, as temperature distribution and overall flame power play a significant role as well. Therefore, the presented setups in parallel can function as a proper tool for the assessment of HT enhancement strategies. As a best practice, the calorimeter is used for large quantity initial testing, and the solid body can be utilized for validation, scale-up, and the derivation of the practical application-relevant temperature distribution. Continued research on HT enhancement strategies and fuel gas variations will be conducted to improve the processes sustainability further. Additional research should focus on the explicability of the observed effects by further experimental evaluation or CFD simulation.

Acknowledgements

The authors express their gratitude to the Linde plc for supplying the gases, hardware, and technological expertise. Specifically, we want to thank the whole department “Manufacturing Markets” and especially the colleagues from the Lindoflamm product line Mr. Marc-Oliver Koerner, Mr. Ronald Steusloff, Mr. Heinz-Dieter Esser, and Mrs. Birgit Himmen. We also appreciate the contribution of Mr. Lukas Fehrenbach and Mr. Michael Pfreuntner with their practical expertise. We acknowledge the received financial support by the StMWi, who granted public funding (AM-EEB; EFP-2003-0007) for this research project through their initiative “Bayrisches Energieforschungsprogramm”.

References

[1] C. D. Donaldson and R. S. Snedeker, "A study of free jet impingement. Part 1. Mean properties of free and impinging jets," *Journal of Fluid Mechanics,* vol. 45, no. 2, pp. 281-319, 1971.

[2] T. S. O'Donovan and D. B. Murray, "Jet impingement heat transfer- Part I: Mean and root-mean-square heat transfer and velocity distributions," *International Journal of Heat and Mass Transfer,* vol. 50, pp. 3291-3301, 2007.

[3] C. D. Donaldson, R. S. Snedeker and D. P. Margolis, "A study of free jet impingement. Part 2. Free jet turbulent structures and impingement heat transfer," *Journal of Fluid Mechanics,* vol. 45, no. 3, pp. 477-512, 1971.

[4] H. Martin, "Heat and Mass Transfer Between Impinging Gas Jets and Solid Surfaces," *Advanced Heat Transfer,* vol. 13, pp. 1-60, 1977.

[5] T. S. O'Donovan and D. B. Murray, "Jet impingement heat transfer- Part II: A temporal investigation of heat transfer and local fluid velocities," *International Journal of Heat and Mass Transfer,* vol. 50, pp. 3302-3314, 2007.

[6] G. K. Hargrave, M. Fairweather and J. K. Kilham, "Forced convective heat transfer from premixed flames- Part 1: Flame structure," *International Journal of Heat and Fluid Flow,* vol. 8, no. 1, pp. 55-63, 1987.

[7] G. K. Hargrave, M. Fairweather and J. K. Kilham, "Forced convective heat transfer from premixed flames- Part 2: Impingement heat transfer," *International Journal of Heat and Fluid Flow,* vol. 8, no. 2, pp. 132-138, 1987.

[8] C. E. Baukal, J. Gebhart and B. Gebhart, "A review of empirical flame impingement heat transfer correlations," *International Journal of Heat and Fluid Flow,* vol. 17, no. 4, pp. 386-396, 1996.

[9] C. E. Baukal and B. Gebhart, "A review of semi-analytical solutions for flame impingement heat transfer," *International Journal of Heat and Mass Transfer,* vol. 39, no. 14, pp. 2989-3002, 1996.

[10] R. Viskanta, "Heat Transfer to Impinging Isothermal Gas and Flame Jets," *Experimental Thermal and Fluid Science,* pp. 111-134, 1993.

[11] S. Chander and A. Ray, "Flame impingement heat transfer: a review," *Energy conversion and management,* vol. 46, no. 18-19, pp. 2803-2837, 2005.

[12] C. J. Hoogendorn, "The effect of turbulence on heat transfer at a stagnation point," *International Journal of Heat and Mass Transfer,* vol. 20, no. 12, pp. 1333-1338, 1977.

[13] T. H. van der Meer, "Stagnation Point Heat Transfer from Turbulent Low Reynolds Number Jets and Flame Jets," *Experimental Thermal and Fluid Science,* vol. 4, no. 1, pp. 115-126, 1991.

[14] H. Herwig and M. G., "The physics of unsteady jet impingement and its heat transfer performance," *Acta Mechanica,* vol. 201, pp. 171-187, 2008.

[15] D. D. Luo, H. S. Zhen, L. C. W. and C. S. Cheung, "Premixed flame impingement heat transfer with induced swirl," *International Journal of Heat and Mass Transfer,* vol. 53, pp. 4333-4336, 2010.

[16] G. Cafiero, G. Castrillo, C. S. Greco and T. Astarita, "Effect of the grid geometry on the convective heat transfer of impinging jets," *International Journal of Heat and Mass Transfer,* vol. 104, pp. 39-50, 2017.

[17] S. Roux, F. M., G. Lalizel, L.-E. Brizzi and E. Dorignac, "Experimental investigation of the flow and heat transfer of an impinging jet under acoustic excitation," *International Journal of Heat and Mass Transfer,* vol. 54, no. 15-16, pp. 3277-3290, 2011.

[18] C. K. Law, A. Makino and T. F. Lu, "On the off-stoichiometric peaking of adiabatic flame temperature," *Combustion and Flame,* vol. 145, pp. 808-819, 2006.

[19] L. L. Dong, C. S. Cheung and C. W. Leung, "Heat transfer characteristics of an impinging butane/air flame jet of low Reynolds number," *Experimental Heat Transfer,* vol. 14, pp. 265-282, 2001.